NASA Technical Paper 2971

January 1990

The Effectiveness of Vane-Aileron Excitation in the Experimental Determination of Flutter Speed by Parameter Identification

E. Nissim

NASA

NASA Technical Paper 2971

1990

The Effectiveness of Vane-Aileron Excitation in the Experimental Determination of Flutter Speed by Parameter Identification

E. Nissim
Ames Research Center
Dryden Flight Research Facility
Edwards, California

National Aeronautics and Space Administration
Office of Management
Scientific and Technical Information Division

CONTENTS

SUMMARY

The effectiveness of aerodynamic excitation is evaluated analytically in this paper in conjunction with the experimental determination of flutter dynamic pressure by parameter identification. Existing control surfaces were used, with an additional vane located at the wingtip. The equations leading to the identification of the equations of motion were reformulated to accommodate excitation forces of aerodynamic origin. The aerodynamic coefficients of the excitation forces do not need to be known since they are determined by the identification procedure. The 12 degree-of-freedom numerical example treated in this work revealed the best wingtip vane locations, and demonstrated the effectiveness of the aileron–vane excitation system. Results from simulated data gathered at much lower dynamic pressures (approximately half the value of flutter dynamic pressure) predicted flutter dynamic pressures with 2-percent errors.

INTRODUCTION

A method has been proposed by Nissim and Gilyard (1989) which allows the prediction of the flutter dynamic pressure from test flights flown far below the flutter dynamic pressure. This prediction is based on the identification of the coefficients of the equations of motion at low dynamic pressures, followed by the solution of these equations to compute the flutter dynamic pressure. The identification stage of the proposed method employs the forced responses of the aircraft, as generated by a set of external sinusoidal forces with constant amplitudes over the entire range of excitation. Nissim and Gilyard (1989) show that proper excitation of the aircraft is required to accurately identify the coefficients and thus the flutter dynamic pressure (Q_F). They give the following guidelines for the external excitation of the aircraft:

1. At least two sets of independent excitation vectors should be used, with a special emphasis on varying the excitation of the rigid body modes so as to yield independent responses.
2. All modes should be excited by the various excitation vectors (although not necessarily by any single vector), keeping the amplitude of the sinusoidal forces constant over the entire range of excitation frequencies.
3. The values of the generalized forces should be such that $F_i/\bar{m}_i$ be of the same order of magnitude for all excited elastic modes, where F_i denotes the ith generalized force and $\bar{m}_i$ denotes the ith generalized mass.
4. The values of $F_i/\bar{m}_i$ associated with the rigid body modes should be approximately two orders of magnitude smaller than those associated with the elastic modes.

These guidelines can be met by inertial forces using eccentric masses, with eccentricities adjusted with the frequency of excitation. These requirements, although theoretically possible, may be difficult to implement on practical configurations. It was therefore decided to investigate other means of excitation, and, in particular, excitation by means of aerodynamic forces.

The feasibility of employing aerodynamic excitation during the experimental determination of the flutter dynamic pressure will be studied in this paper. The identification equations of Nissim and Gilyard (1989) will be modified to accommodate excitation by means of aerodynamic surfaces. The formulated method does not require knowledge of the aerodynamic coefficients associated with the exciting control surfaces since they are identified by the described experimental procedure. The method is subsequently tested on NASA's drone for aerodynamic and structural testing–aerodynamic research wing 2 (DAST–ARW2) mathematical model (Adams and Tiffany, 1985). This model comprises 12 modes (two rigid body modes and ten elastic modes). Aerodynamic excitation will be achieved by means of the existing aileron and an added wingtip vane.

NOMENCLATURE

DAST–ARW2	drone for aerodynamic and structural testing–aerodynamic research wing 2
EA	elastic axis
g	acceleration or structural damping
HL	hinge line
L.E.	leading edge
m	number of excitation vectors
$\bar{m}_i$	ith generalized mass
n	number of modes
n_c	number of active aerodynamic excitation surfaces
Q	dynamic pressure
Q_D	flight dynamic pressure
T	transpose
t	time
V	flight speed
WT	weighting
α	vane rotation angle
β	aileron rotation angle
γ	elevon rotation angle
ρ	air density
ω	frequency of oscillation
ω_F	flutter frequency

Matrixes

$[B]$	defined in equation (11)
$[C]$	defined in equation (3)
$[\bar{C}]$	damping matrix
$[\bar{F}_A]$	defined in equation (3)
$[\bar{\bar{F}}_A]$	aerodynamic coefficients of exciting surfaces
$[F_0]$	defined in equation (7)
$[\bar{F}_0]$	defined in equation (4)
$[F_1]$	defined in equation (7)
$[\bar{F}_1]$	defined in equation (4)

NOMENCLATURE

DAST–ARW2	drone for aerodynamic and structural testing–aerodynamic research wing 2
EA	elastic axis
g	acceleration or structural damping
HL	hinge line
L.E.	leading edge
m	number of excitation vectors
$\bar{m}_i$	ith generalized mass
n	number of modes
n_c	number of active aerodynamic excitation surfaces
Q	dynamic pressure
Q_D	flight dynamic pressure
T	transpose
t	time
V	flight speed
WT	weighting
α	vane rotation angle
β	aileron rotation angle
γ	elevon rotation angle
ρ	air density
ω	frequency of oscillation
ω_F	flutter frequency

Matrixes

$[B]$	defined in equation (11)
$[C]$	defined in equation (3)
$[\bar{C}]$	damping matrix
$[\bar{F}_A]$	defined in equation (3)
$[\bar{\bar{F}}_A]$	aerodynamic coefficients of exciting surfaces
$[F_0]$	defined in equation (7)
$[\bar{F}_0]$	defined in equation (4)
$[F_1]$	defined in equation (7)
$[\bar{F}_1]$	defined in equation (4)

$[K]$	defined in equation (3)
$[\bar{K}]$	stiffness matrix
$[\bar{M}]$	mass matrix
$[q]$	response amplitudes
$[q_0]$	response matrix
$[T]$	defined in equation (10)
$[\delta]$	amplitudes of rotations of the exciting aerodynamic surfaces

Subscripts

E	exact
F	flutter
I	imaginary
nf	number of frequencies of excitation
R	real

IDENTIFICATION OF THE EQUATIONS OF MOTION

Let the equations of motion be given by

$$[\bar{M}][\ddot{q}_0] + [\bar{C}][\dot{q}_0] + [\bar{K}][q_0] = [\bar{\bar{F}}_A][\delta]e^{i\omega t} \tag{1}$$

where $[\bar{M}]$, $[\bar{C}]$, and $[\bar{K}]$ denote respectively the mass, damping, and stiffness matrixes of the aircraft and include the aerodynamic contributions to the equations of motion (Nissim and Gilyard, 1989). The matrix $[\bar{\bar{F}}_A]$ denotes the aerodynamic coefficients matrix associated with the excitation surfaces. Matrix $[\delta]$ denotes the amplitudes of rotation of the exciting aerodynamic surfaces and ω denotes the frequency of excitation.

Note that matrixes $[\bar{M}]$, $[\bar{C}]$, and $[\bar{K}]$ are all real and are of order $n \times n$, where n is the number of degrees of freedom of the system. The response matrix $[q_0]$ is complex and is of the order $n \times m$, where m represents the number of excitation vectors. Matrix $[\bar{\bar{F}}_A]$ is of the order $n \times n_c$, where n_c denotes the number of aerodynamic surfaces used for excitation. Matrix $[\delta]$ is an $n_c \times m$ matrix denoting the deflections of the exciting aerodynamic surfaces.

Premultiplying equation (1) by $[\bar{M}]^{-1}$ and substituting

$$[q_0] = [q]e^{i\omega t}$$

yields the following equation

$$(-\lceil I \rfloor\omega^2 + [C]i\omega + [K])[q] = [\bar{F}_A][\delta] \tag{2}$$

where

$$\begin{aligned} [C] &= [\bar{M}]^{-1}[\bar{C}] \\ [K] &= [\bar{M}]^{-1}[\bar{K}] \\ [\bar{F}_A] &= [\bar{M}]^{-1}[\bar{\bar{F}}_A] \end{aligned} \tag{3}$$

and where $\lceil I \rfloor$ denotes the unit matrix.

Following the assumptions made by Nissim and Gilyard (1989) regarding the form of the aerodynamic coefficients, matrix $[\bar{F}_A]$ can be written in the form

$$[\bar{F}_A] = \frac{1}{2}\rho V^2[\bar{F}_0] + \frac{1}{2}\rho V[\bar{F}_1]i\omega \tag{4}$$

Hence, equation (2) can be written as

$$(-\lceil I \rfloor\omega^2 + [C]i\omega + [K])[q] = Q_D[\bar{F}_0][\delta] + i\omega\frac{Q_D}{V}[\bar{F}_1][\delta] \tag{5}$$

where $Q_D = \frac{1}{2}\rho V^2$.

It is now assumed that the excitation frequency, the responses, and the control deflections are all measured with the objective of identifying the real matrixes $[C]$, $[K]$, $[\bar{F}_0]$, and $[\bar{F}_1]$. Assume the system is excited with frequencies $\omega_1, \omega_2, \ldots, \omega_{nf}$ using aerodynamic surface deflections $[\delta]_1, [\delta]_2, \ldots, [\delta]_{nf}$, with resulting responses $[q]_1, [q]_2, \ldots, [q]_{nf}$. Equation (5) can then be written in the form

$$\begin{aligned}
[C]i\omega_1[q]_1 + [K][q]_1 - [F_0][\delta]_1 - [F_1]i\omega_1[\delta]_1 &= \omega_1^2[q]_1 \\
[C]i\omega_2[q]_2 + [K][q]_2 - [F_0][\delta]_2 - [F_1]i\omega_2[\delta]_2 &= \omega_2^2[q]_2 \\
&\vdots \\
[C]i\omega_{nf}[q]_{nf} + [K][q]_{nf} - [F_0][\delta]_{nf} - [F_1]i\omega_{nf}[\delta]_{nf} &= \omega_{nf}^2[q]_{nf}
\end{aligned} \tag{6}$$

where

$$\begin{aligned}
[F_0] &= Q_D[\bar{F}_0] \\
[F_1] &= \frac{Q_D}{V}[\bar{F}_1]
\end{aligned} \tag{7}$$

Equation (6) can be written in a compact form after transposing it, that is

$$\begin{bmatrix}
[q]_1^{\mathrm{T}} & i\omega_1[q]_1^{\mathrm{T}} & -[\delta]_1^{\mathrm{T}} & -i\omega_1[\delta]_1^{\mathrm{T}} \\
[q]_2^{\mathrm{T}} & i\omega_2[q]_2^{\mathrm{T}} & -[\delta]_2^{\mathrm{T}} & -i\omega_2[\delta]_2^{\mathrm{T}} \\
\vdots & & & \\
[q]_{nf}^{\mathrm{T}} & i\omega_{nf}[q]_{nf}^{\mathrm{T}} & -[\delta]_{nf}^{\mathrm{T}} & -i\omega_{nf}[\delta]_{nf}^{\mathrm{T}}
\end{bmatrix}
\begin{bmatrix}
[K]^{\mathrm{T}} \\ [C]^{\mathrm{T}} \\ [F_0]^{\mathrm{T}} \\ [F_1]^{\mathrm{T}}
\end{bmatrix}
=
\begin{bmatrix}
\omega_1^2[q]_1^{\mathrm{T}} \\ \omega_2^2[q]_2^{\mathrm{T}} \\ \vdots \\ \omega_{nf}^2[q]_{nf}^{\mathrm{T}}
\end{bmatrix} \tag{8}$$

where T denotes the transpose matrix.

Equation (8) can be written as

$$[T]\begin{bmatrix}
[K]^{\mathrm{T}} \\ [C]^{\mathrm{T}} \\ [F_0]^{\mathrm{T}} \\ [F_1]^{\mathrm{T}}
\end{bmatrix} = [B] \tag{9}$$

where

$$[T] = \begin{bmatrix}
[q]_1^{\mathrm{T}} & i\omega_1[q]_1^{\mathrm{T}} & -[\delta]_1^{\mathrm{T}} & -i\omega_1[\delta]_1^{\mathrm{T}} \\
[q]_2^{\mathrm{T}} & i\omega_2[q]_2^{\mathrm{T}} & -[\delta]_2^{\mathrm{T}} & -i\omega_2[\delta]_2^{\mathrm{T}} \\
\vdots & & & \\
[q]_{nf}^{\mathrm{T}} & i\omega_{nf}[q]_{nf}^{\mathrm{T}} & -[\delta]_{nf}^{\mathrm{T}} & -i\omega_{nf}[\delta]_{nf}^{\mathrm{T}}
\end{bmatrix} \tag{10}$$

and where

$$[B] = \begin{bmatrix} \omega_1^2 [q]_1^T \\ \omega_2^2 [q]_2^T \\ \vdots \\ \omega_{nf}^2 [q]_{nf}^T \end{bmatrix} \tag{11}$$

Following the discussion of Nissim and Gilyard (1989), a constraint is now imposed on the matrix coefficients to be identified, forcing all of them to be real. In this latter case, equation (9) can be written as

$$\begin{bmatrix} T_R \\ T_I \end{bmatrix} \begin{bmatrix} [K]^T \\ [C]^T \\ [F_0]^T \\ [F_1]^T \end{bmatrix} = \begin{bmatrix} B_R \\ B_I \end{bmatrix} \tag{12}$$

where as before (Nissim and Gilyard, 1989)

$$[B] = [B_R] + i[B_I] \tag{13}$$

and

$$[T] = [T_R] + i[T_I] \tag{14}$$

The difference between the aerodynamic excitation equations and those using constant amplitude vectors (Nissim and Gilyard, 1989) manifests itself in the form assumed by matrix $[T]$. The aerodynamic excitation appears to present more flexibility since the deflections of the aerodynamic surfaces $[\delta]$ can be varied at every frequency of excitation, whenever such a variation is deemed necessary. This is contrary to the formulation presented in Nissim and Gilyard (1989) whereby the excitation vectors had to be kept constant, except for vector multipliers which could be accommodated in the analysis. The number of unknowns is larger in the present formulation since in addition to $[F_0]^T$, one has to determine also $[F_1]^T$. However, the added number of unknowns is relatively small and is not expected to present any difficulties from a numerical point of view (that is, $2(n + n_c)$ unknowns here, compared to $2n + n_c$ in Nissim and Gilyard (1989)). Matrixes $[K]$ and $[C]$ are used to compute the predicted flutter speed following the solution of equation (12), for two different flight dynamic pressures (Nissim and Gilyard, 1989). Matrixes $[F_0]$ and $[F_1]$, however, are never used in determining the predicted flutter dynamic pressure.

PRESENTATION AND DISCUSSION OF RESULTS

Numerical Example

As previously stated, the DAST–ARW2 mathematical model was used to test the effectiveness of the aerodynamic excitation. It consists of two rigid body modes (plunge and pitch) and ten elastic symmetric modes. Figure 1 shows the locations of the three existing control surfaces: the aileron, close to the tip of the wing; the all-moving elevon, and the flaperon. A wingtip vane was added to these existing control surfaces. Figure 2 shows the root locus plot of the basic DAST–ARW2 model, with zero structural damping ($g = 0$) and without the addition of the wingtip vane. In this root locus plot, as in all the root locus plots in this work, the value of the dynamic pressure Q_D is varied between 0 and 650 lb/ft^2, with 25 lb/ft^2 increments. The flutter dynamic pressure is $Q_F = 487$ lb/ft^2 and the flutter frequency $\omega_F = 117$ rad/sec (fig. 2). The elastic modes natural frequencies range from 49.3 rad/sec for the first wing bending, to approximately 492 rad/sec for the highest elastic mode.

Addition of a Wingtip Vane

According to Nissim and Gilyard (1989), at least two linearly independent excitation vectors are required for a reasonably accurate identification of the aircraft. Therefore, for the present work, at least two control surfaces must be used to form these independent excitation vectors. Since the basic flutter mechanism involves the wing bending and torsion modes, the excitation vectors should be able to excite the wing modes particularly well. Since the flaperon is too close to the root of the wing (fig. 1) for it to be the second excitation surface, a wingtip vane was added. The vane together with the aileron will yield the basic contributions to the two linearly independent excitation vectors. It should be mentioned that the use of wingtip vanes for aerodynamic excitation is not new, and the experience obtained from their usage so far has been very favorable (Koenig, 1981).

Figure 3 shows the wing with a vane added at its tip, with the vane's leading edge (L.E.) aligned with the L.E. of the wing. This vane will be referred to as vane 1, and its dimensions are 3.25-in. chord and 7-in. span. Figure 4 shows the root locus plot of the DAST–ARW2 model with the added vane 1. The addition of the vane led to a substantial reduction in the flutter dynamic pressure, yielding Q_F = 435 lb/ft^2 and ω_F = 121 rad/sec. It was therefore decided to reduce the size of the vane while maintaining its L.E. aligned with the L.E. of the wing. The smaller vane will be referred to as vane 2, with dimensions of 2.275-in. chord and 2.5-in. span. The DAST–ARW2 model with vane 2 added is shown in figure 5. The root locus plots for this configuration (not shown in this report) yielded Q_F = 465 lb/ft^2 and ω_F = 118 rad/sec. An alternative location for the vane was sought since such a reduction in Q_F is undesirable while introducing an excitation vane.

Vane 3 was located along the wingtip so that its root quarter chord point coincided with the elastic axis (EA) of the wing (approximately 44 percent of the wingtip chord). The size of vane 3 was modified to lie between the sizes of vane 1 and vane 2, and it was also tapered. The vane dimensions are 2-in. root chord, 1.2-in. tip chord, and 5-in. span. At this location, vane 3 yielded Q_F = 496 lb/ft^2 and ω_F = 122 rad/sec. Although the increase in flutter speed is very small in relation to the vaneless wing value of Q_F (= 487 lb/ft^2) the condition number of matrix $[T]$ started to show a substantial increase. This is because as the vane is moved toward the trailing edge, its associated forcing vector becomes more similar to the aileron forcing vector, leading to a deterioration in the condition number of matrix $[T]$. Therefore vane 3 was moved upstream 1 in. This vane, referred to as vane 4, is shown in figure 6. At this location, vane 4 has its root quarter chord point 1 in. upstream of the EA, at the 35.8-percent wingtip chord location. The resulting values for Q_F and ω_F are given by Q_F = 485 lb/ft^2 and ω_F = 122 rad/sec.

Table 1 summarizes the numerical results for flutter dynamic pressures and frequencies associated with the different vanes. The best vane location for purposes of aerodynamic excitation, with minimum effects on the flutter dynamic pressure, is when the vane quarter chord point is slightly upstream of the EA, approximately 35 percent of the wingtip chord.

All the results shown from here on will relate to vane 4. For the sake of completeness, the root locus plot associated with vane 4 is presented in figure 7. Figure 7(a) is obtained using $g = 0$ (zero structural damping), and figure 7(b) is obtained using $g = 0.03$, yielding Q_F = 493 lb/ft^2 and ω_F = 123 rad/sec.

The root locus plots presented so far (figs. 2, 4, and 7) were derived using lifting surface aerodynamics at Mach 0.86, with aerodynamics expanded into Padé approximates using four lag terms. This same form of 'exact' aerodynamics is also used to calculate the simulated responses needed to identify the equations of motion (see eq. (12)). The identification stage uses approximations of the exact aerodynamics which, from the results presented by Nissim and Gilyard (1989), appear to retain the essential features necessary for the determination of the flutter dynamic pressure.

Finally, all the simulated responses calculated for identification are derived assuming 3-percent structural damping; that is, $g = 0.03$. Hence, the exact values of Q_F and ω_F to be identified by the proposed experimental procedure, and denoted by an added subscript E, are given in figure 7(b); that is, $(Q_F)_E$ = 493 lb/ft^2 and $(\omega_F)_E$ = 123 rad/sec. These values, with figure 7(b), will form the reference for comparison with the experimentally predicted results. All

identifications will be performed at $Q = 150$ lb/ft^2 and at $Q = 250$ lb/ft^2, and the results obtained will be used to calculate the predicted flutter dynamic pressure. Unless otherwise stated, the excitation frequency range will span the values between 0.5 and 550 rad/sec with 750 excitation frequencies.

Results Obtained Using Vane–Aileron Excitation and Exact Responses

Vane and aileron aerodynamic excitations will be presented in this section. The first objective is to determine the amplitude of deflection of the vane relative to the amplitude of the aileron. This relative deflection has the effect of giving different weights to the vane responses relative to the aileron responses during the least-square solution of equation (12).

Let α, β, and γ denote the deflections, in radians, of the vane, aileron, and elevon, respectively. A series of identification runs were made using the following form of $[\delta]$

$$[\delta] = \begin{bmatrix} \alpha \\ \beta \end{bmatrix} = \begin{bmatrix} \alpha_1 & \alpha_2 \\ \beta_1 & \beta_2 \end{bmatrix} = \begin{bmatrix} X & 0 \\ 0 & 0.02 \end{bmatrix} \tag{15}$$

and with varying values for X (which is associated with the vane deflection). The value of 0.02 for the aileron deflection was chosen since it represents approximately 1° deflection. These results, which relate to exact non-contaminated responses, are summarized in table 2. It can be seen that the best value for X is 0.08 and that the differences between the predicted values of Q_F are small. In the following, the value of $X = 0.08$ will be used in conjunction with the aileron angle $\beta_2 = 0.02$. In some cases, where smaller vane angles are preferable, $X = 0.04$ can be chosen with essentially the same accuracy for Q_F (approximately 8-percent error in all cases). Figure 8(a) shows the root locus plot of the identified system with $X = 0.08$. This plot is similar to figure 7(b) which represents the exact system.

The simultaneous excitation of the aileron and vane was then attempted and shown to yield essentially the same results as those obtained by the separate excitation of the vane–aileron surfaces. Figure 8(b) shows one such result obtained using

$$[\delta] = \begin{bmatrix} \alpha \\ \beta \end{bmatrix} = \begin{bmatrix} 0.08 & 0.08 \\ 0.02 & -0.02 \end{bmatrix}$$

Finally, it was necessary to get an idea of the amplitudes of rotation of the aileron and of the vane required to obtain reasonable responses. To do this, the maximum accelerations in g were computed for $Q = 150$ lb/ft^2 and for $Q = 250$ lb/ft^2. These results are shown in figures 9(a) and 9(b). As these figures show, the above small angles of rotation lead to peak accelerations of 8 g, except for the very high frequencies where the vane excitation (± 0.08 rad) leads to acceleration levels in the range of 14–18 g. This indicates that very small angles of rotation will be sufficient for both vane and aileron excitations.

Results Obtained Using Vane–Aileron–Elevon Excitation and Exact Responses

Results will be presented using two forcing vectors involving the simultaneous excitation of vane–elevon and aileron–elevon surfaces and results using three forcing vectors (vane–aileron–elevon rotations). The elevon rotations were chosen to lie within the range of values which lead to changes in the sign of the identified rigid body pitch force (as obtained from the identified solution for $[F_0]$) to ensure linearly independent rigid body excitation. The results obtained are summarized in table 3. The effects of the added elevon lead to a very small reduction in the error values associated with Q_F (approximately 1 percent). Therefore, there is no need to excite the aircraft by any surface other than the vane and aileron surfaces.

Attempts will be made in the following to reduce the errors in the predicted values of Q_F and to find the effects of response contaminations on the predicted values of Q_F. For this purpose, the following vane–aileron rotations will be assumed throughout the remainder of this work.

$$[\delta] = \begin{bmatrix} \alpha \\ \beta \end{bmatrix} = \begin{bmatrix} 0.08 & 0 \\ 0 & 0.02 \end{bmatrix}$$

Results Using Weighted Least-Square Solutions

The results in this report show errors in Q_F which appear to be higher than those in Nissim and Gilyard (1989). It was suspected that these errors occurred because the amplitude of the aerodynamic forces of excitation decrease as the frequency of excitation increases. A two-dimensional wing oscillating at high values of reduced frequency yields aerodynamic coefficients with half the absolute values of those associated with very low reduced frequencies (Bisplinghoff, Ashley, and Halfman, 1955). It was therefore decided to counteract this fall in the aerodynamic coefficients by weighting equation (12). The following form of weighting $WT(\omega)$ was used in producing the results described as

$$\begin{aligned} WT(\omega) &= \text{FREQC} \;\; ; \;\; \omega \leq \text{FREQC} \\ WT(\omega) &= \text{FREQC} + (\omega - \text{FREQC}) * \text{SLOPE} \;\; ; \;\; \omega > \text{FREQC} \end{aligned} \tag{16}$$

where FREQC = constant and SLOPE = constant.

To counteract the reduction of the aerodynamic coefficients with frequency increase, FREQC and SLOPE were assigned the values FREQC = 1 and SLOPE = 0.002. In the frequency range of excitation (between 0.5 and 550 rad/sec), this yields approximately twice as much weight to the high frequency equations as the low frequency equations. The results are summarized in table 4. Improved results are obtained, with errors of approximately 5 percent.

The 5-percent random errors in the responses lead to a change of only 0.4 percent in Q_F. The introduction of additional errors in the measurements of the rotations of the aerodynamic surfaces (also 5-percent random errors) lead to an additional error of 0.4 percent in Q_F. As formulated by Nissim and Gilyard (1989) and herein, the method is robust to errors. An example of a root locus plot using contaminated responses and rotations (case 3 in table 4) is shown in figure 10.

Identification of the Elastic Equations Only

In Nissim and Gilyard (1989), the rigid body modes present numerical difficulties in the identification of the equations of motion. For flutter problems where rigid body modes affect the dynamic behavior at flutter, the previously mentioned procedure for the experimental determination of the flutter dynamic pressure can be pursued. However, for those cases where flutter involves elastic modes only, with negligible effect of the rigid body modes, one may wish to identify the elastic equations only and discard the rigid body modes. To restate this in more definite terms, assume that all the modes are identified and measured. Ignore the rigid body responses and feed into equation (10) only those responses associated with the elastic modes. The frequency range of excitation is changed to start at higher frequency values, preferably near the first elastic natural frequency. This change helps avoid unnecessary errors caused by the coupling terms between rigid body modes and elastic modes at the low frequencies (where the rigid body responses are particularly large). The results presented so far have used a frequency excitation range of 0.5 to 550 rad/sec. In the following, three ranges will be used for the identification of only the elastic equations: 30 to 550 rad/sec, 40 to 550 rad/sec, and 50 to 550 rad/sec. It should be noted that the value of the first natural elastic frequency is 49.3 rad/sec.

The results obtained using the previously mentioned procedure are summarized in table 5. The best results are obtained with the frequency range of 50 to 550 rad/sec, yielding Q_F = 517 lb/ft^2 and ω_F = 116 rad/sec. This result for Q_F is 4.9 percent higher than the exact value. Figure 11 shows the root locus plot associated with the 50 to 550 rad/sec frequency range, which is similar to the exact root locus plot (fig. 7(b)).

The effects of the weighted least-square solution of the identification equations were tested on the computed flutter dynamic pressure and flutter frequency. The effects of contaminating the various rotations and responses (with 5-percent random errors) were also tested. The results obtained are summarized in table 6.

The weighted least-square solution with FREQC = 1 and with SLOPE = 0.002, using exact responses and rotations, yields Q_F = 502 lb/ft^2 and ω_F = 113 rad/sec, with the error in Q_F approximately 1.8 percent. Contamination of the responses and rotations has a negligible effect on Q_F (0.2 percent each). Figure 12 shows the root locus plot associated with the most contaminated data (case 3 in table 6).

Finally, case 1 (table 6) was tested again, but with a single forcing vector consisting of the aileron only. Although the values obtained for Q_F and ω_F show reasonable errors, with Q_F = 537 lb/ft^2 (that is, 8.9-percent error) and ω_F = 116 rad/sec, the root locus plot shown in figure 13 indicates that the overall dynamic behavior of the identified system is indeed different from that of the exact system.

CONCLUDING REMARKS

Aerodynamic excitation by means of an aileron and a wingtip vane provides a very good excitation system for the experimental determination of the flutter dynamic pressure by parameter identification. The results indicate that:

1. The best vane location along the tip of the wing is around the point where the vane's root quarter chord point is slightly ahead of the wing's elastic axis. Placing of the vane too far upstream leads to a substantial reduction in the wing's flutter dynamic pressure. Placing of the vane too far downstream causes the vane's forcing vector to be too similar to the aileron's forcing vector, leading to potential numerical difficulties.

2. Small vane and aileron rotations yield large responses, allowing large response-to-noise ratios during test flights.

3. Simultaneous excitation of the vane and the aileron is not needed. Separate excitation using each surface individually is sufficient.

4. Constant amplitudes of vane and aileron rotations were used to produce the results obtained, with analytical weighting done during the analysis of the results. This doesn't mean, however, that rotational amplitudes cannot be changed during the frequency sweep, since the measured responses can be normalized with respect to a desired constant vane or aileron rotational angle. Any desired level of excitation can be chosen during the test to ensure the best response to noise ratios.

5. The most accurate values for the flutter dynamic pressure (approximately 2-percent error) were obtained by the identification of the elastic equations only. The rigid body responses were discarded and the range of frequencies of excitation was reduced.

6. In all cases treated in this work, the errors in the predicted flutter dynamic pressure did not exceed 9 percent. Ways of reducing the errors to approximately 2 percent were treated in the body of this work.

7. Contamination of responses and of excitation surface rotations by 5-percent random errors had negligible effects (less than 1 percent) on Q_F.

REFERENCES

Adams, W., and S. Tiffany, "Development of a Flutter Suppression Control Law by Use of Linear Quadratic Gaussian and Constrained Optimization Design Techniques," 2nd International Symposium on Aeroelasticity and Structural Dynamics, West Germany, Apr. 1985.

Bisplinghoff, R.L., H. Ashley, and R.L. Halfman, *Aeroelasticity*, Addison-Wesley Publishing Co., 1955.

Koenig, K., "Experience from Flight Flutter Testings With Tip Vanes on Airbus," International Symposium on Aeroelasticity, Nuremberg, West Germany, Oct. 1981.

Nissim, E., and Glenn B. Gilyard, *Method for Experimental Determination of Flutter Speed by Parameter Identification*, NASA TP-2923, 1989.

Table 1. Flutter dynamic pressures and flutter frequencies for the different vanes tested.

Vane number	Q_F, lb/ft^2	ω_F, rad/sec	HL,[a] percent
1	435	121	6.4
2	465	118	4.5
3	496	122	43.8
4	485	122	35.8
No vane	487	117	—

[a]HL: Hinge location of the vane along the wingtip's chord (in percent of wingtip chord). The hinge is located at the root quarter chord point of the vane.

Table 2. Identified flutter dynamic pressures and flutter frequencies for different values of vane excitation angles X[a], with aileron excitation angle = 0.02 rad.

X, rad/sec	Q_F, lb/ft^2	ω_F, rad/sec	$\frac{\Delta Q_F}{(Q_F)_E}$, percent error
0.04	533	118	8.1
0.08	530	118	7.5
0.12	533	119	8.1
0.16	536	121	8.7

[a]X defined as

$$[\delta] = \begin{bmatrix} \alpha \\ \beta \end{bmatrix} = \begin{bmatrix} X & 0 \\ 0 & 0.02 \end{bmatrix}$$

Table 3. Identified flutter dynamic pressures and flutter frequencies using simultaneous excitation of vane–elevon and aileron–elevon.

Case[a]	Q_F, lb/ft^2	ω_F, rad/sec	$\frac{\Delta Q_F}{(Q_F)_E}$, percent error
1	525	118	6.5
2	523	117	6.1
3	524	117	6.3
4	527	117	6.9

[a]Case 1: $[\delta] = \begin{bmatrix} \alpha \\ \beta \\ \gamma \end{bmatrix} = \begin{bmatrix} 0.08 & 0 \\ 0 & 0.02 \\ -0.002 & -0.002 \end{bmatrix}$

Case 2: $[\delta] = \begin{bmatrix} \alpha \\ \beta \\ \gamma \end{bmatrix} = \begin{bmatrix} 0.08 & 0 \\ 0 & 0.02 \\ -0.004 & -0.004 \end{bmatrix}$

Case 3: $[\delta] = \begin{bmatrix} \alpha \\ \beta \\ \gamma \end{bmatrix} = \begin{bmatrix} 0.08 & 0 \\ 0 & 0.02 \\ -0.001 & -0.0025 \end{bmatrix}$

Case 4: $[\delta] = \begin{bmatrix} \alpha \\ \beta \\ \gamma \end{bmatrix} = \begin{bmatrix} 0.08 & 0 & 0 \\ 0 & 0.02 & 0 \\ 0 & 0 & 0.002 \end{bmatrix}$

Table 4. Identified values of flutter dynamic pressures and flutter frequencies using weighted solution of the least-square equation.

Case[a]	Q_F, lb/ft^2	ω_F, rad/sec	$\frac{\Delta Q_F}{(Q_F)_E}$, percent error
1	514	114	4.3
2	516	114	4.7
3	518	115	5.1

[a]Cases 1, 2, 3:

$$[\delta] = \begin{bmatrix} \alpha \\ \beta \end{bmatrix} = \begin{bmatrix} 0.08 & 0 \\ 0 & 0.02 \end{bmatrix},$$

FREQC = 1, SLOPE = 0.002.

Case 1: Identification using exact responses.

Case 2: Identification using responses contaminated with 5-percent random errors.

Case 3: Identification using responses and aerodynamic surface rotations contaminated with 5-percent random errors.

Table 5. Identified values of flutter dynamic pressures and flutter frequencies using exact elastic responses only (with rigid body responses discarded).

Case[a]	Q_F, lb/ft^2	ω_F, rad/sec	$\frac{\Delta Q_F}{(Q_F)_E}$, percent error
1	526	117	6.7
2	521	117	5.7
3	517	116	4.9

[a]Cases 1, 2, 3:

$$[\delta] = \begin{bmatrix} \alpha \\ \beta \end{bmatrix} = \begin{bmatrix} 0.08 & 0 \\ 0 & 0.02 \end{bmatrix},$$

SLOPE = 0.

Case 1: Excitation frequency range 30 to 550 rad/sec.

Case 2: Excitation frequency range 40 to 550 rad/sec.

Case 3: Excitation frequency range 50 to 550 rad/sec.

Table 6. Identified values of flutter dynamic pressures and flutter frequencies using weighted least-square solution and elastic responses only.

Case[a]	Q_F, lb/ft^2	ω_F, rad/sec	$\frac{\Delta Q_F}{(Q_F)_E}$, percent error
1	502	113	1.8
2	501	112	1.6
3	503	113	2.0

[a]Cases 1, 2, 3:

$$[\delta] = \begin{bmatrix} \alpha \\ \beta \end{bmatrix} = \begin{bmatrix} 0.08 & 0 \\ 0 & 0.02 \end{bmatrix},$$

FREQC = 1, SLOPE = 0.002, excitation range 50 to 550 rad/sec.

Case 1: Identification using exact responses.

Case 2: Identification using responses contaminated with 5-percent random errors.

Case 3: Identification using responses and aerodynamic surface rotations contaminated with 5-percent random errors.

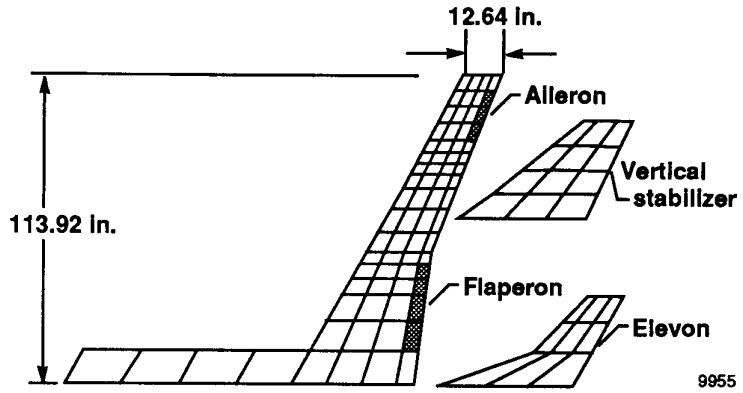

Figure 1. The DAST–ARW2 aerodynamic model and aerodynamic paneling.

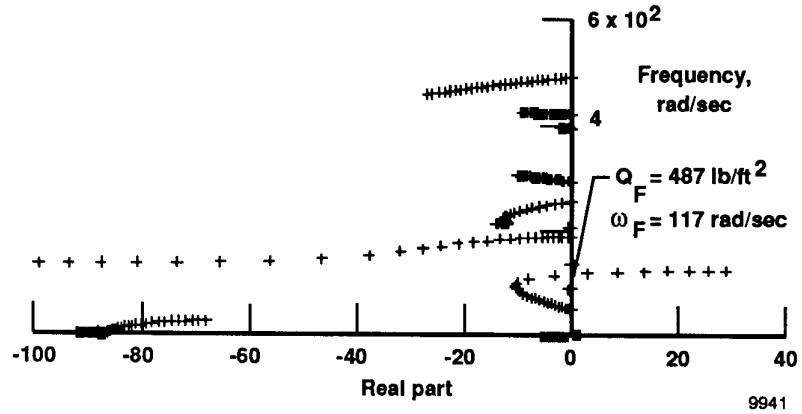

Figure 2. Root locus plot of DAST–ARW2 mathematical model with no vanes ($g = 0$).

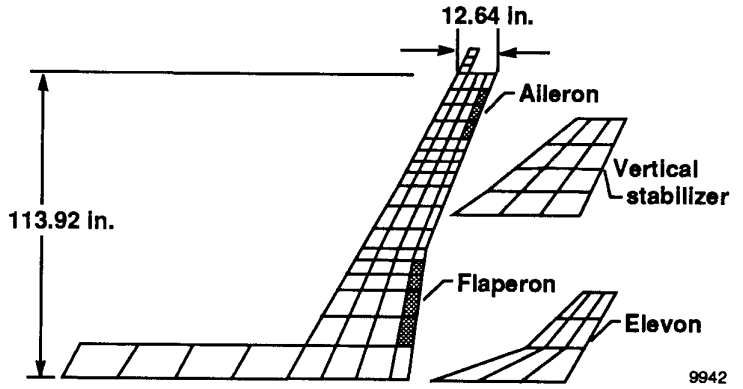

Figure 3. The DAST–ARW2 aerodynamic model with vane 1 and aerodynamic paneling.

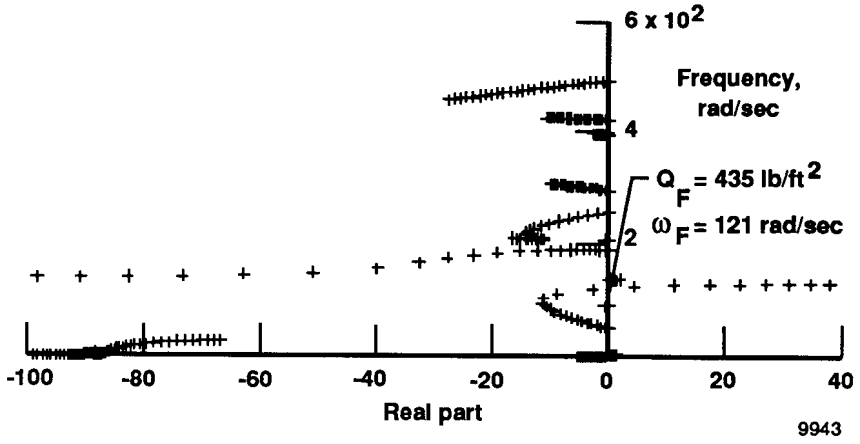

Figure 4. Root locus plot of DAST–ARW2 mathematical model with vane 1 ($g = 0$).

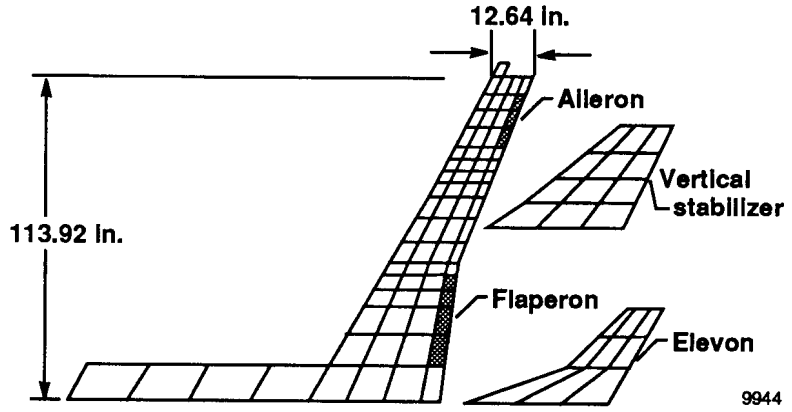

Figure 5. The DAST–ARW2 aerodynamic model with vane 2 and aerodynamic paneling.

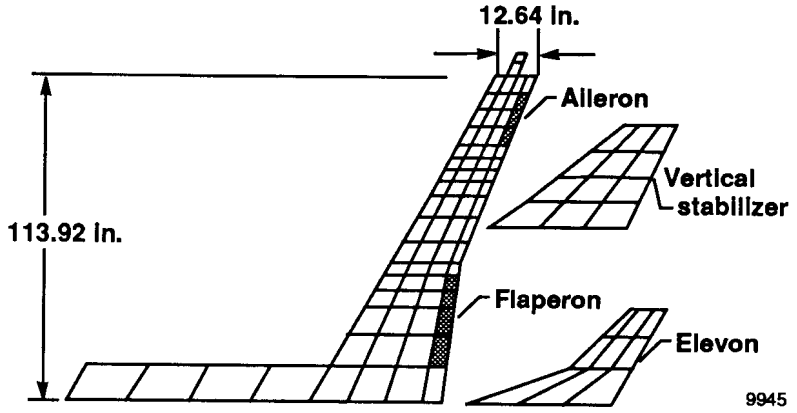

Figure 6. The DAST–ARW2 aerodynamic model with vane 4 and aerodynamic paneling.

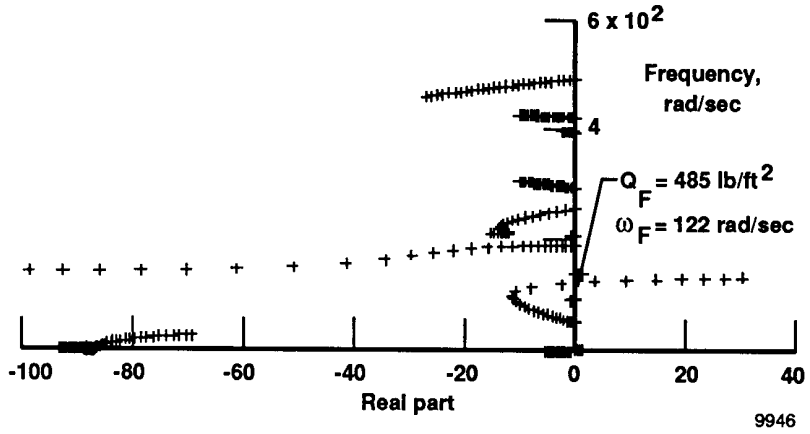

(a) $g = 0$.

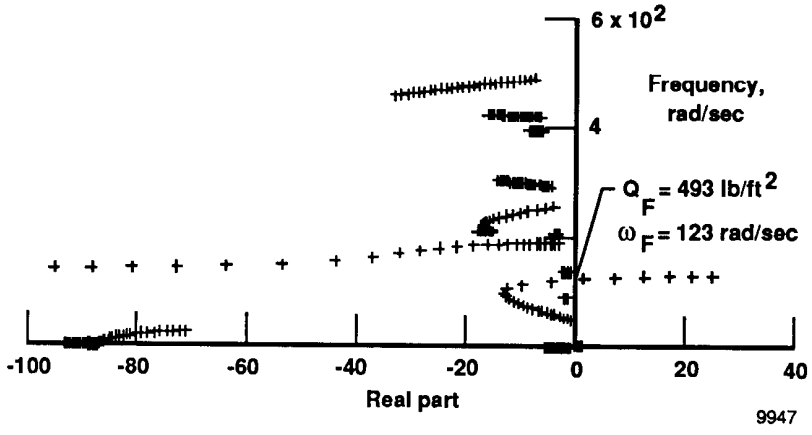

(b) $g = 0.03$.

Figure 7. Root locus plot of DAST–ARW2 mathematical model with vane 4.

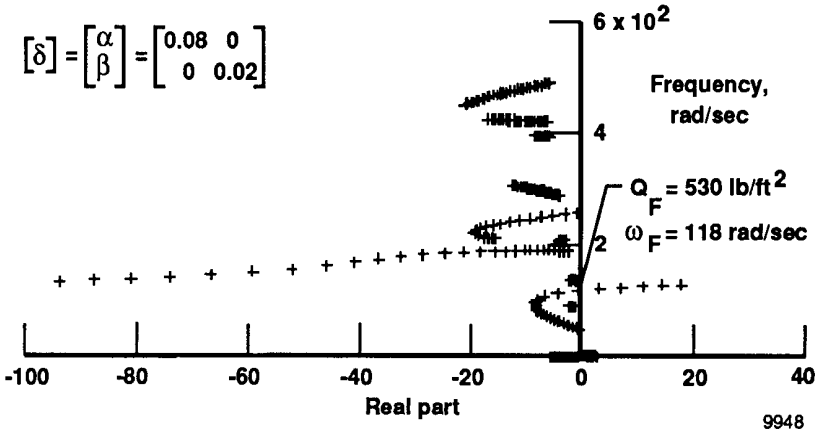

(a) $[\delta] = \begin{bmatrix} \alpha \\ \beta \end{bmatrix} = \begin{bmatrix} 0.08 & 0 \\ 0 & 0.02 \end{bmatrix}$.

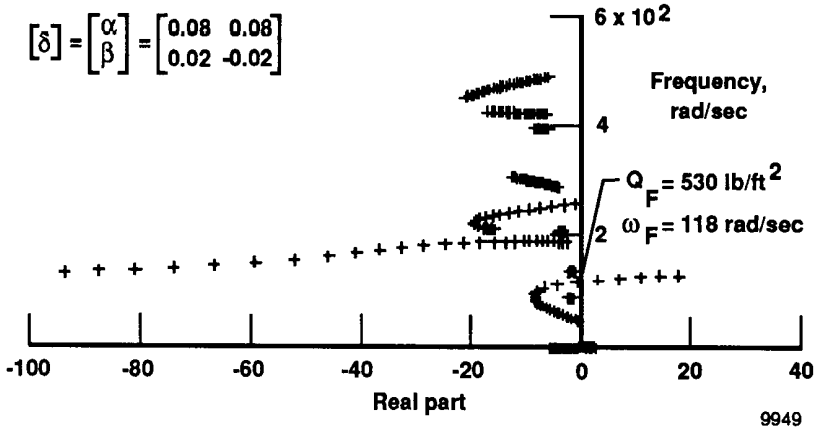

(b) $[\delta] = \begin{bmatrix} \alpha \\ \beta \end{bmatrix} = \begin{bmatrix} 0.08 & 0.08 \\ 0.02 & -0.02 \end{bmatrix}$.

Figure 8. Root locus plot using exact responses.

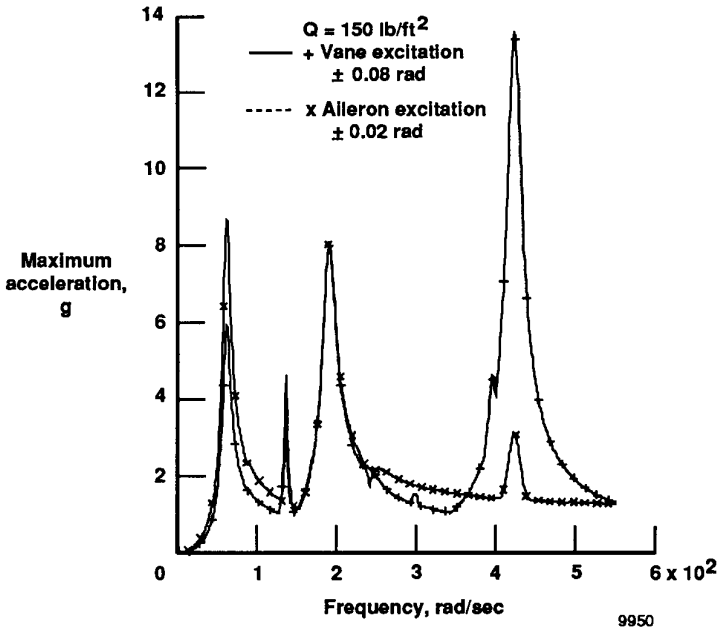

(a) Q = 150 lb/ft^2.

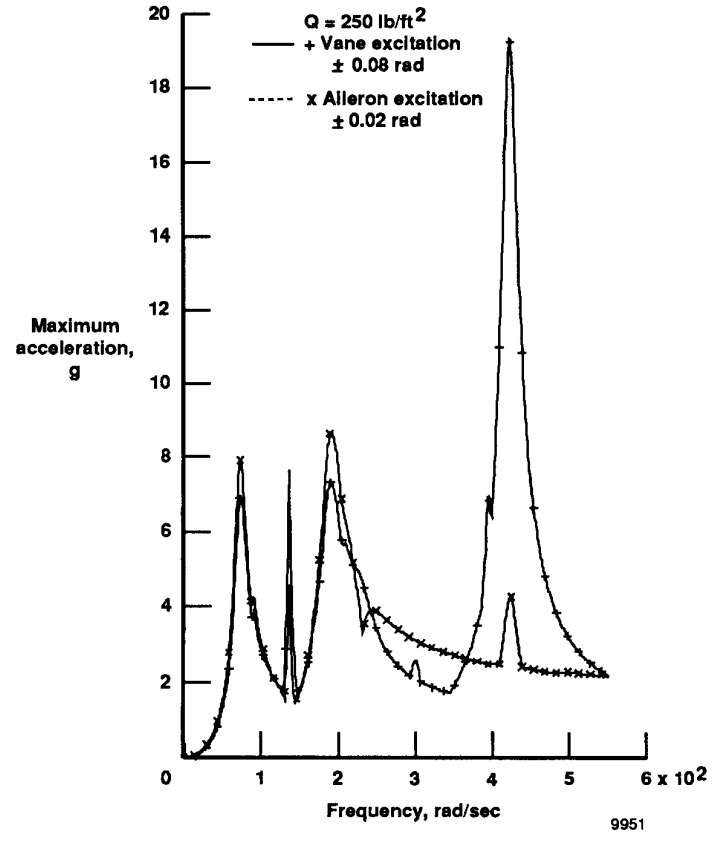

(b) Q = 250 lb/ft^2.

Figure 9. Maximum absolute accelerations at various frequencies using aileron or vane excitation.

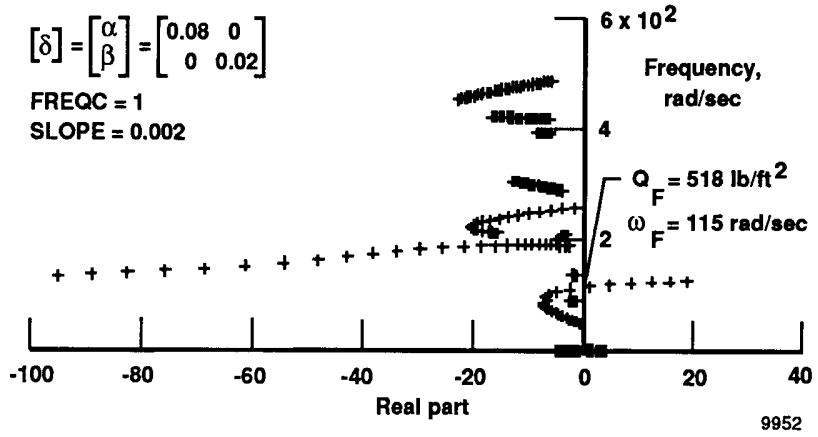

Figure 10. Root locus plot using 5-percent random errors in response and rotations.

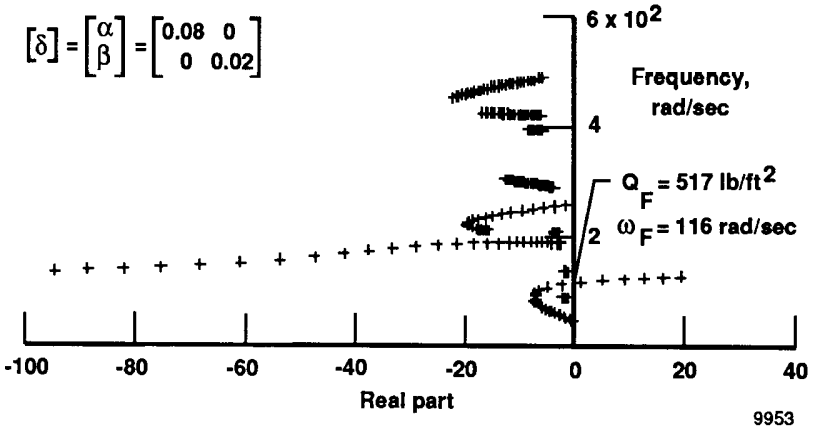

Figure 11. Root locus plot using exact simulated responses of elastic modes with an excitation range of 50 to 550 rad/sec.

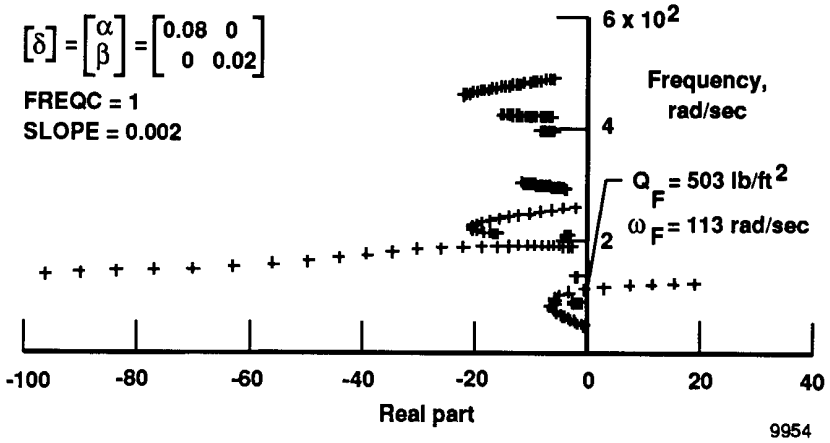

Figure 12. Root locus plot using contaminated responses of elastic modes and [δ] rotations (5-percent random errors for both).

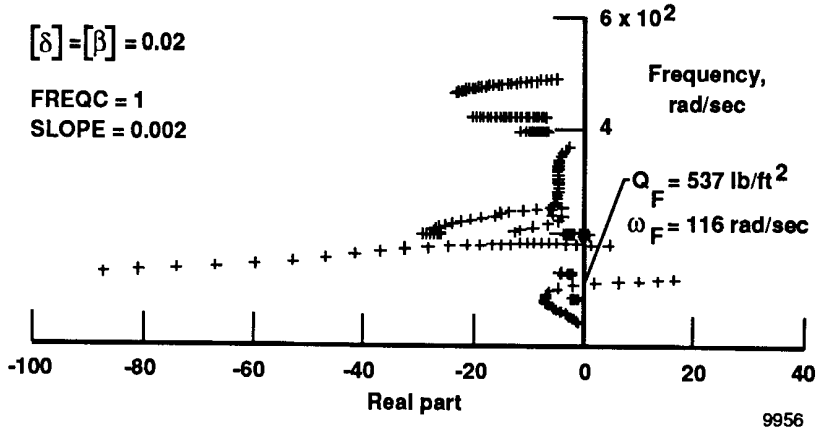

Figure 13. Root locus plot using exact responses of elastic modes with an excitation range of 50 to 550 rad/sec.

NASA National Aeronautics and Space Administration

Report Documentation Page

1. Report No.	2. Government Accession No.	3. Recipient's Catalog No.
NASA TP- 2971		

4. Title and Subtitle

The Effectiveness of Vane-Aileron Excitation in the Experimental Determination of Flutter Speed by Parameter Identification

5. Report Date

January 1990

6. Performing Organization Code

7. Author(s)

E. Nissim

8. Performing Organization Report No.

H-1516

10. Work Unit No.

RTOP 505-66-71

9. Performing Organization Name and Address

NASA Ames Research Center
Dryden Flight Research Facility
P.O. Box 273, Edwards, CA 93523-5000

11. Contract or Grant No.

13. Type of Report and Period Covered

Technical Paper

12. Sponsoring Agency Name and Address

National Aeronautics and Space Administration
Washington, DC 20546

14. Sponsoring Agency Code

15. Supplementary Notes

This research was undertaken while Eli Nissim held a National Research Council – NASA (Ames Research Center, Dryden Flight Research Facility) Research Associateship. The author was on leave from Technion – Israel Institute of Technology.

16. Abstract

The effectiveness of aerodynamic excitation is evaluated analytically in this paper in conjunction with the experimental determination of flutter dynamic pressure by parameter identification. Existing control surfaces were used, with an additional vane located at the wingtip. The equations leading to the identification of the equations of motion were reformulated to accommodate excitation forces of aerodynamic origin. The aerodynamic coefficients of the excitation forces do not need to be known since they are determined by the identification procedure. The 12 degree-of-freedom numerical example treated in this work revealed the best wingtip vane locations, and demonstrated the effectiveness of the aileron–vane excitation system. Results from simulated data gathered at much lower dynamic pressures (approximately half the value of flutter dynamic pressure) predicted flutter dynamic pressures with 2-percent errors.

17. Key Words (Suggested by Author(s))	18. Distribution Statement
Flutter testing Parameter identification	Unclassified — Unlimited Subject category 05

19. Security Classif. (of this report)	20. Security Classif. (of this page)	21. No. of pages	22. Price
Unclassified	Unclassified	24	A02

NASA FORM 1626 OCT 86

**For sale by the National Technical Information Service, Springfield, VA 22161-2171.*

NASA-Langley, 1990